

Dry Excess Electrons in Room-Temperature Ionic Liquids


Claudio J. Margulis,^{*,†} Harsha V. R. Annapureddy,[†] Pablo M. De Biase,[†] David Coker,^{‡,§} Jorge Kohanoff,^{||} and Mario G. Del Pópolo^{||}

[†]Department of Chemistry, University of Iowa, Iowa City, Iowa 52241, United States

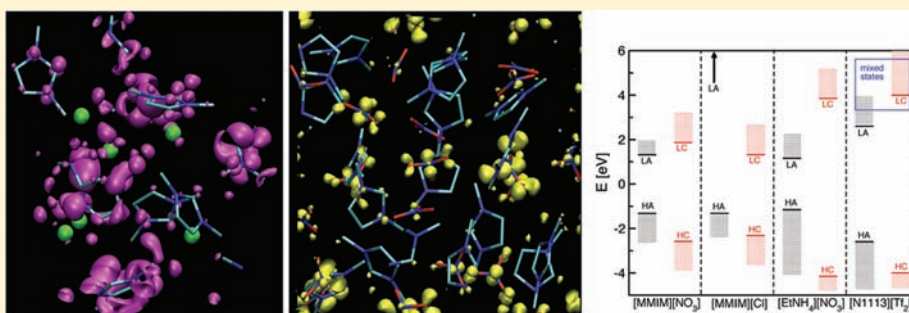
^{*}Department of Physics, University College Dublin, Dublin 4, Ireland

[§]Department of Chemistry, Boston University, Boston, Massachusetts 02215, United States

^{||}Atomistic Simulation Centre, School of Mathematics and Physics, Queen's University Belfast, Belfast BT7 1NN, U.K.

 Supporting Information

ABSTRACT:



In this article, we describe general trends to be expected at short times when an excess electron is generated or injected in different room-temperature ionic liquids (RTILs). Perhaps surprisingly, the excess electron does not localize systematically on the positively charged cations. Rather, the excess charge localization pattern is determined by the cation and anion HOMO/LUMO gaps and, more importantly, by their relative LUMO alignments. As revealed by experiments, the short-time (ps/ns) transient UV spectrum of excess electrons in RTILs is often characterized by two bands, a broad band at low energies (above 1000 nm) and another weaker band at higher energies (around 400 nm). Our calculations show that the dry or presolvated electron spectrum (fs) also has two similar features. The broad band at low energies is due to transitions between electronic states with similar character on ions of the same class but in different locations of the liquid. The lower-intensity band at higher energies is due to transitions in which the electron is promoted to electronic states of different character, in some cases on counterions. Depending on the chemical nature of the RTIL, and especially on the anions, excess electrons can localize on cations or anions. Our findings hint at possible design strategies for controlling electron localization, where electron transfer or transport across species can be facilitated or blocked depending on the alignment of the electronic levels of the individual species.

1. INTRODUCTION

Room temperature ionic liquids (RTILs) have been extensively investigated as solvents for cleaner radioactive material processing¹ and as electrolytes for electrochemical devices such as supercapacitors and solar cells.² Under standard operation conditions, these applications lead naturally to the interaction of the molten salt with highly reducing excess electrons that might have deleterious effects on the materials' properties. Although this is a topic of fundamental and practical interest, the interaction between excess electrons and RTILs is not yet fully understood, and a faithful microscopic description of solvated and presolvated electrons in these complex organic salts is still missing.

Since electrons are light, reactions of solvated electrons in conventional solvents are known to be at least an order of magnitude faster than reactions of the hydrogen radical. However, the

opposite has been observed in certain RTILs, where the reaction of the hydrogen radical has been measured to be 20 times faster.^{3,4} It is conceivable that the ionic nature of RTILs plays an important role in the kinetics and localization behavior of electrons. The long lifetimes of solvated electrons in some RTILs combined with their slow, viscous molecular dynamics may have important implications in radiation chemistry.

Many years of experimental work on the radiation chemistry of RTILs have provided a wealth of information on degradation products and radiolytic pathways. As Wishart recently pointed out,⁵ dry electron capture by solutes at modest concentrations can have a significant impact on the radiation damage of the solvent, and since RTILs can often dissolve both polar and

Received: April 13, 2011

Published: October 27, 2011

nonpolar molecules, pulse radiolysis and photodetachment experiments in RTILs provide an opportunity to study such intermediate species.⁵ These experiments can also help us gain a better understanding of electronic transport and transfer as well as the chemistry of the species involved, which are subjects of great interest in energy storage and other technological applications such as recycling of spent nuclear fuel.

In the present work, we used electronic structure calculations to study the initial state of an excess electron in a series of RTILs equilibrated before irradiation. The spectra and patterns of localization are necessarily those of the initial transient species since the electron has not yet been solvated by the liquid (i.e., it is in the dry electron state). To keep our conclusions as general as possible, we investigated a wide variety of systems, ranging from a perfect crystal and several liquids to small clusters and ion pairs in the gas phase. Motivated by a series of thorough experimental studies available in the literature,^{3,5–18} we primarily focused on imidazolium (e.g., [mmim⁺]) and alkylammonium (e.g., [N₁₁₁₃⁺])-based ILs.

Wang et al.^{19,20} used first-principles molecular dynamics (MD) simulations to investigate the presolvation of electrons in dimethylimidazolium and 1-methylpyridinium chloride ([mmim][Cl] and [1-MPy][Cl]). They reported that shortly after injection, the excess electron is delocalized over the unoccupied manifold of cationic π orbitals. This agrees with the intuitive idea that before a convenient cavity is formed in the liquid, the electron should interact preferably with the positively charged molecules.

This appealing idea, however, is challenged by the calculations presented here. While these interesting findings apply to the above systems, they are not completely general, and as we will show in the subsequent sections, there are several other RTILs where the excess electron delocalizes over *anions*. Our results indicate that the crucial ingredient for rationalizing the excess electron localization pattern is not whether the electron prefers positive or negative ions or whether the cations are aromatic or aliphatic but instead the relative alignment of cationic and anionic electronic states in the liquid phase. For example, in the case of [Cl⁻], its first empty level appears at very high energies, which means that practically any system involving [Cl⁻] has the excess electron localized on the unoccupied orbitals of the cations or in cavities in the liquid. Replacing [Cl⁻] with [NO₃⁻] results in the appearance of lower-lying empty anionic states that, depending on the counterion, may lie below cation states. A clear understanding of this phenomenon opens the possibility of tailoring systems in which an excess electron can be forced to localize on cations or anions and where transfer and transport across species can be blocked or facilitated.

2. METHODS

To understand the patterns of localization of excess electrons in RTILs, we conducted electronic structure calculations in the condensed phase and in the gas phase for a range of different systems. The liquid phase of ethyltrimethylammonium bis(trifluoromethane)sulfonimide ([N₁₁₁₃][Tf₂N]) was modeled with a periodically replicated box containing eight ion pairs (304 atoms), while finite size effects were assessed with a system of 32 ion pairs (1216 atoms). Ethylammonium nitrate ([C₂H₅][NH₃][NO₃]) in the liquid state was modeled with 20 ion pairs (300 atoms), and the crystalline²¹ phase was modeled using an X-ray structure provided by P. C. Trulove, whose monoclinic unit cell contains 8 ion pairs (120 atoms).²¹ The liquid phases of [mmim][Cl] and

[mmim][NO₃] were studied using systems of 8 (136 atoms) and 20 ion pairs (400 atoms), respectively.

To gain further understanding of the commonalities and differences among these systems and a better appreciation of the origin of certain features in the experimental UV spectra, periodic calculations were supplemented with calculations for increasingly large clusters, ranging from one to eight ion pairs for [N₁₁₁₃][Tf₂N] and up to 24 pairs for [(C₂H₅)NH₃][NO₃]. Such clusters were still treated under periodic boundary conditions, but the size of the simulation box was chosen to be large enough that the interaction between periodic replicas was negligible. This was particularly important when the excess electron was added to the cluster.

In the case of [mmim][Cl], our results in the liquid phase come from snapshots collected from equilibrated first-principles MDs simulations without the excess electron.²² For [N₁₁₁₃][Tf₂N], [(C₂H₅)NH₃][NO₃], and [mmim][NO₃], configurations for clusters and the liquid phase were generated using appropriate empirical force fields. To correct for small bond length differences between the classical and first-principles descriptions, and for consistency across systems, all of the configurations were energy-minimized by first-principles methods at the same level of theory.

The bulk of the first-principles calculations were carried out using the SIESTA code.^{23,24} This code implements density functional theory (DFT) calculations within the generalized gradient approximation (GGA) using a flexible basis set of numerical orbitals. The core electrons are replaced with norm-conserving pseudopotentials. Periodic boundary conditions are automatically taken into account by expanding the electron density in plane waves on a regular grid commensurate with the periodic box and computing the electrostatic contributions to the energy and potential using Fourier transforms. The basis functions are pseudoatomic orbitals obtained by solving the Kohn–Sham equations for the isolated atom, represented by the pseudopotential rather than the bare coulomb interaction. In the present calculations, we used the PBE functional²⁵ and a double- ζ plus polarization (DZP) basis set, amounting to 13 orbitals for first-row atoms and five orbitals for the hydrogen atoms. Following usual practice with SIESTA, we imposed a strict confinement of the basis functions that forced them to become zero beyond a species- and angular-momentum-dependent radius determined by the condition that the eigenvalues were all upshifted by 25 meV with respect to the unconfined atom.

The most critical calculations were repeated at the more expensive hybrid DFT–Hartree–Fock B3LYP level^{26–28} using Gaussian basis sets (3-21G*). These calculations were carried out using the CP2K package,^{29,30} which also implements periodic boundary conditions. The reason for going beyond pure DFT approaches was the suspicion that the excess electron, being unpaired in the singly occupied molecular orbital, could be the subject of important self-interaction effects.³¹ In agreement with the results of calculations on excess electrons in water, it turned out that such effects were unimportant.³² Self-interaction appears to be more relevant in positively charged systems generated by the removal of an electron and creation of a hole.³³ The second reason for carrying out the more expensive hybrid calculations was the well-known underestimation of the valence–conduction energy band gap by pure DFT approaches. This is relevant to the calculation of the optical absorbance spectrum, and we will expand on this point in section 3.3. In the case of [N₁₁₁₃][Tf₂N] ion pairs, the results obtained using SIESTA were verified against ab initio calculations at the MP2 level obtained using the Gaussian software.³⁴ The patterns of electron localization were found to be very similar in these two cases.

The dry or presolvated excess electron and hole dielectric response line spectrum of [N₁₁₁₃][Tf₂N] was computed using SIESTA.^{24,23} The spectrum was broadened with a Gaussian function of 1 eV fwhm at the location of each peak. This broadening value, though somewhat arbitrary, is reasonable on the basis of prior careful analysis of the

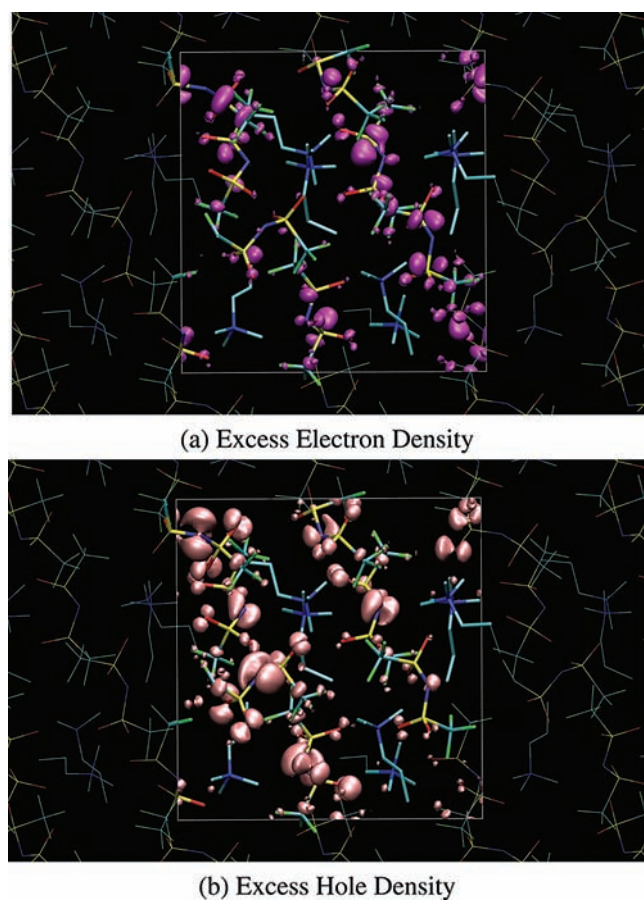


Figure 1. (a) $(\rho_- - \rho_0)$ and (b) $(\rho_0 - \rho_+)$ for the $[N_{1113}][Tf_2N]$ system. The number of grid-point divisions along x , y , and z is 80, and the isosurface value is $0.004744 \text{ e}/\text{\AA}^3$.

electronic and thermal orbital energy fluctuations in condensed-phase systems.^{35–37}

The nature of the eigenstates in all of our studied systems, whether cation- or anion- localized or of mixed character, was determined by projecting the Kohn–Sham orbitals onto the atomic basis functions and discriminating between anionic and cationic centers. In a nonminimal, nonorthogonal basis set such as the DZP basis set used here, such a projection is never pure. However, in the present case of ionic systems, covalent bonding is a secondary feature, and the eigenstates are anion- or cation-localized to a very large extent. To fix a criterion, we chose to label a state as *cationic* when its projection on cations was larger than 70% (and likewise for anionic). This assignment was confirmed visually by inspecting the three-dimensional spatial distribution of the associated Kohn–Sham orbital.

3. RESULTS

3.1. Condensed-Phase Electron-Density Difference Distributions. Understanding electron localization or delocalization in RTILs is important in order to rationalize patterns of reactivity. A feature common to several RTILs discussed in section 3.3 is the transient appearance of two bands in the absorption spectrum. A broad peak appears at low energies, which is similar to what is commonly observed in the spectra of solvated electrons in conventional liquids, and another less prominent peak is noticeable at higher energies. In a recent article, Shkrob and Wishart³⁸

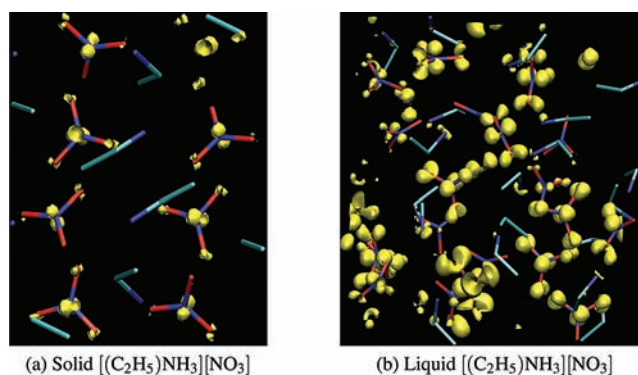


Figure 2. Density differences $(\rho_- - \rho_0)$ for $[(C_2H_5)NH_3][NO_3]$ in its (a) crystalline phase²¹ and (b) liquid phase. The isosurface value was set to $0.004744 \text{ e}/\text{\AA}^3$ in the case of the liquid and $0.032 \text{ e}/\text{\AA}^3$ in the case of the solid. The density grid for solid $[(C_2H_5)NH_3][NO_3]$ was set to 54, 60, and 54 points in x , y , and z , respectively. For the liquid, the grid was set to 80 points in all directions.

suggested that the species absorbing on the high-energy side of the spectrum in imidazolium-based liquids may be a dimeric radical cation. This sort of insight is not yet available for alkylammonium-based systems. Whether these two peaks are due to the absorption of different species or the same species is not yet fully understood, and in section 3.3 we attempt to address this issue, at least on the very short (fs) time scale, for the case of the dry electron and hole.

Since in DFT the total electron density of the system is a meaningful quantity, in order to understand the transient patterns of localization of the excess electron, we computed $(\rho_- - \rho_0)$, the electron-density difference between a negatively charged ($Q_{\text{total}} = -1$) and a neutral $[N_{1113}][Tf_2N]$ liquid snapshot. For the same liquid configuration, we also computed $(\rho_0 - \rho_+)$, the electron-density difference between the neutral and positively charged ($Q_{\text{total}} = +1$) systems. Visualization of these density differences allows us to understand the early patterns of localization of an excess electron and an excess hole in the $[N_{1113}][Tf_2N]$ system. Calculations were performed on several independent configurations with similar results.

Figure 1a,b clearly shows that at time $t = 0$ after irradiation, the dry excess electron and excess hole are localized on the $[Tf_2N^-]$ anions. The density difference in these plots is shown only for a central box, but it should be understood that this box is periodically replicated. Simple visual inspection reveals that the localization of the excess electron is mostly away from the N atom at the geometrical center of the $[Tf_2N^-]$ anion and generally appears on the S and O atoms. On the contrary, the excess hole appears to be localized mostly at the center of $[Tf_2N^-]$ on the N and O atoms. Interestingly, our calculations showed that structural relaxation via energy minimization of both liquid- and gas-phase $[N_{1113}][Tf_2N]$ in the presence of an excess electron leads to the decomposition of an $[Tf_2N^-]$ anion. While the results of a simple minimization may not be indicative of the predominant long-time chemical bond-breaking pathways, ample evidence for the decomposition of this anion upon excess electron injection exists.^{13,39–41}

It is instructive to compare the pattern of localization of an excess electron in $[N_{1113}][Tf_2N]$ with that in other very different RTILs. Figure 2a,b shows the electron-density differences for the crystalline and liquid phases of $[(C_2H_5)NH_3][NO_3]$. Perhaps

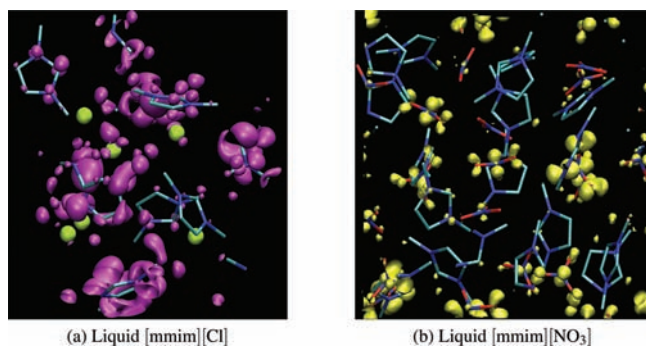


Figure 3. Density differences ($\rho_- - \rho_0$) for (a) liquid [mmim][Cl] and (b) liquid [mmim][NO₃]. In all cases, the isosurface value was set to 0.004744 e/Å³ and the grids were set to have 80 divisions along *x*, *y*, and *z*. The Cl⁻ ions in (a) appear as green spheres, and the NO₃⁻ anions in (b) correspond to the red-and-blue structures.

more interesting is a comparison of the localization patterns in [mmim][Cl] and [mmim][NO₃]. In agreement with the work of Wang and co-workers,^{19,20} we find that for [mmim][Cl] the excess charge appears localized on the *aromatic* cations. However, the result appears to be different for [mmim][NO₃], where for the same cations at the level of theory used in this work, the dry electron localizes more over the anions. This is shown in Figure 3a,b. A note of caution should be raised in the case of [mmim][NO₃] because the cationic and anionic conduction bands are close in energy, and small geometrical differences may result in charge localization over cations, anions, or mixed ionic states. We find that in this particular system, the excess charge localization is very dependent on minimization to adjust the liquid force-field geometries to the ab initio potential energy surface.

Therefore, it is not the aromatic or aliphatic nature of the cation that dictates the patterns of localization. The origin of this phenomenon is more subtle and is related to the alignment of electronic energy levels in the liquid, as will be discussed in detail in section 3.2.

3.2. Electronic Energies and a Rationale for the Patterns of Excess Electron Localization. Since the structure of the [(C₂H₅)NH₃⁺] cation is fairly simple and the crystal structure of [(C₂H₅)NH₃][NO₃] is known,²¹ we chose this system for an in-depth analysis of the electronic structure in the presence and absence of an excess electron. We studied a sequence of increasingly large gas-phase clusters as they transition toward the liquid and the crystal. The top panel of Figure 4 shows the Kohn–Sham energy levels of neutral systems, taking the HOMO as the reference. Next to each level we have indicated its ionic character as cationic (C) or anionic (A), as defined in section 2. In this way, we have characterized the HOMO and lowest-lying unoccupied MOs for neutral systems ranging from an ion-pair dimer (two ion pairs) to the liquid and solid states. It is clear that in the case of [(C₂H₅)NH₃][NO₃], the HOMO and the lowest unoccupied states are always anionic. This analysis predicts where a dry excess electron will localize and also permits us to estimate the magnitude of thermal electronic dispersion within bands of states that have the same electronic character. For example, we see that in the liquid, the lowest band of empty anionic states spans a range of ~1 eV, whereas the same band is narrower in the solid and in the clusters.

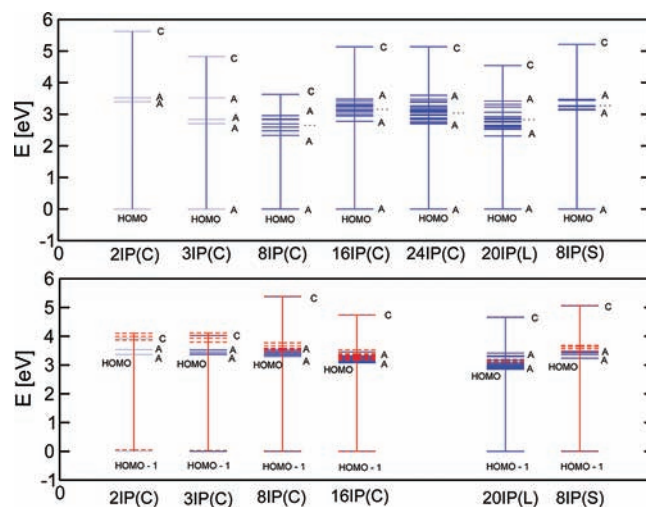


Figure 4. (top) Electronic energy levels of neutral clusters (C) and the liquid (L) and solid (S) phases of [(C₂H₅)NH₃][NO₃]. (bottom) Energy levels for the same systems in the presence of an excess electron. Notation: *n*IP stands for *n* ion-pairs, and the letter A or C next to each horizontal line indicates whether the corresponding state is *anionic* or *cationic* according to the criterion specified in section 2. Red and blue correspond to spin-up and spin-down states.

The bottom panel of Figure 4 shows the electronic energy levels for the same systems in the presence of an excess electron ($Q_{\text{total}} = -1$) without further optimization of the geometry. Red and blue lines correspond to different spin states. To provide a clearer comparison with the neutral system (top panel), in this case the reference energy was defined as that of the HOMO–1, which corresponds to the HOMO of the neutral system. Just as in the case of the condensed-phase [N₁₁₁₃][Tf₂N] system, the excess electron is clearly localized on the anions. An interesting observation is the pattern of localization of the HOMO and lowest-lying unoccupied MOs in comparison with those in the absence of the excess electron. In all of the thermally disordered states (liquid and clusters), the presence of the excess electron results in a narrower conduction band.

The energy diagrams in Figure 4 can indeed help in rationalizing the zero-time absorption spectrum of dry electrons and holes in different RTILs. In section 3.3 we will discuss our computed absorbance spectrum in the case of [N₁₁₁₃][Tf₂N], which for the solvated electron is experimentally known.⁴² Some of the features in this spectrum are generic to many different ILs. The transient absorbance spectrum of excess electrons in RTILs often shows a broad peak at low energies followed by a smaller and narrower band at higher energies. What in section 3.3 will be called *translational electronic transitions* correspond to transitions between the HOMO (occupied by the excess electron, located at ~3 eV in the lower panel in the case of [(C₂H₅)NH₃][NO₃]) and the nearby LUMOs in the same band, which possess identical anionic character (in other systems, the HOMO and nearby LUMOs may be cationic). For the dry electron, this gives rise to the low-energy absorption band. On the other hand, the peak commonly observed at high energy can be associated, at least in part, with transitions from the HOMO to higher-energy unoccupied states of different character (the next band up). As an example, in the case of [(C₂H₅)NH₃][NO₃] we predict that higher-energy transitions from an anionic HOMO to cationic unoccupied states that are ~2 eV higher in energy should occur.

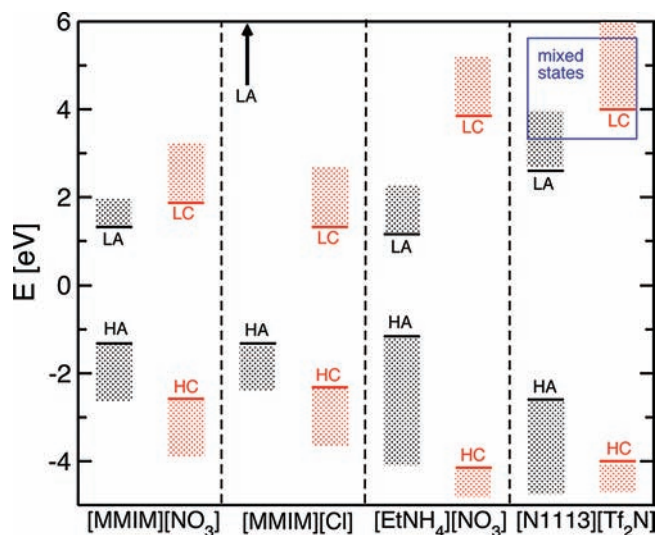


Figure 5. HOMOs and LUMOs of cations and anions in the four RTIL systems investigated in this paper. Electronic energy levels (horizontal lines) were calculated on liquid samples. Vertical boxes showing the extent of cationic and anionic states are schematic. The abbreviations LA/LC and HA/HC denote anion/cation LUMO and anion/cation HOMO, respectively. The vertical arrow in the [mmim][Cl] panel indicates that the anion's LUMO is off the scale of the graph. The square box in the [N₁₁₁₃][Tf₂N] panel indicates that over that particular energy window electronic states have a mixed anionic–cationic character.

This energy gap between states of different character is RTIL-dependent, as can be appreciated from Figure 5. Of course, the results presented in section 3.3 should be interpreted as valid only at $t = 0$. Since at $t = 0$ the liquid is transparent over the energy range probed, only transitions from the excess electron or excess hole can contribute to the $t = 0$ dry electron/hole spectrum. Currently available experiments probe the spectrum at longer time scales, where chemistry may have already occurred and other absorbing species such as radicals could contribute to the spectrum.

The condensed-phase electronic energy levels adjust self-consistently in such a way that the neutral liquid LUMO can be located on either cations or anions, independent of the HOMO/LUMO gap of the isolated ions. It is therefore crucial to emphasize that it is not the cation's or anion's HOMO/LUMO gap alone that determines the character of the state occupied by an excess electron. Instead, this is determined by the relative energy alignment of cationic and anionic states in the condensed phase, which is not predictable from the properties of the isolated ions because it depends on the local electrostatic field created by the environment. This is better understood by analyzing the behavior of different RTILs. Figure 5 shows the alignment of cation and anion states in the neutral liquid phase for each of the systems studied here. Specifically, we recognize that the HOMO of the neutral liquid is always associated with the anions. However, and perhaps surprisingly, except in the case of [mmim][Cl], the LUMO of each liquid studied here is also associated with the anions. This means that tentatively, in all of our RTILs except [mmim][Cl], an excess dry electron should be localized on the anions. Clearly [mmim][Cl] is different not because of the cation but because of the large condensed-phase HOMO/LUMO gap in [Cl⁻]. Interestingly, in the case of the neutral [mmim][NO₃] liquid, the lowest unoccupied cationic

states are quite close in energy to the LUMO band, which has anionic character. It is plausible that small fluctuations in the liquid may favor localization on cations, anions, or significantly mixed states. This means that careful modification of the cation's or anion's chemical structure may enable control of the species on which initial electron localization occurs.

Two important considerations should be made regarding the effect of the system length and time scales on the final fate of excess electrons in RTILs. First, electron localization in interstitial cavities offering the appropriate dielectric environment should not be disregarded, particularly when enough reorganization occurs in the liquid after electron injection or for systems large enough that such cavities may appear spontaneously. Ultimately, a balance between the large kinetic energy of confinement and Coulombic stabilization should be established in order to have a bound state in a cavity. This type of analysis is beyond the scope of the current work, since our systems were prepared such that they would be in equilibrium before the generation of electrons.

The second point to consider is what happens to the liquid upon addition of an excess electron in terms of local structural reorganization. For example, it is experimentally known that the [NO₃⁻] anion undergoes chemical reactions to form a dianion in the condensed phase.¹⁸

3.3. Interpretation of the Dry Electron Spectrum. The steady-state and transient spectra of the solvated electron in imidazolium- and alkylammonium-based ILs have been measured by different groups. Funston and Wishart⁹ have also compared the absorption spectra of excess electrons measured in [N₁₄₄₄][Tf₂N] and many other conventional solvents and shown that the broad part of the spectrum at low energies is quite similar to what is observed in diamines or acetonitrile. Interestingly, although the high-energy region appears to be quite similar when the alkylammonium cation is replaced by methylbutylpyrrolidinium, the broad peak at lower energies is quite sensitive to the particular nature of the aliphatic cation.⁹ In the case of [N₁₄₄₄][Tf₂N], the high-energy peak appears at ~400 nm and the broad low-energy band at ~1400 nm.³ Wishart has shown that the lifetimes of these two peaks in the transient spectrum of [N₁₄₄₄][Tf₂N] are different.⁵ The broad feature peaking at ~1400 nm decays as a first-order process with a lifetime of 170–300 ns, while the smaller peak at high energies decays with a shorter lifetime of ~50 ns. In contrast to the low-energy peak, no reactivity of the species giving rise to this peak was observed in the presence of electron scavengers.⁵ Because of this observation, the peak at high energy was tentatively assigned to the absorption of the radical [NTf₂*].⁵

Katoh et al.⁴² found similar features in the transient spectrum of the much less viscous [N₁₁₁₃][Tf₂N] system. Consistent with what was previously observed, changing the identity of the cation modified the location of the low-energy peak, which in this case was located at ~1000 nm, while the peak at higher energies was still found at ~400 nm.

Detailed analysis of the short-time transient spectrum of several different imidazolium-based RTILs with halogen anions⁴³ has shown the same two features at low and high energies (a broad peak at ~1500 nm and a small, sharper peak at 700–800 nm).

Figure 6 shows our dry electron spectrum for [N₁₁₁₃][Tf₂N] computed from the imaginary part of the dielectric function generated by SIESTA.^{23,24} A similar computation performed on the same RTIL without the excess electron shows, as expected, that [N₁₁₁₃][Tf₂N] is optically transparent in the range of

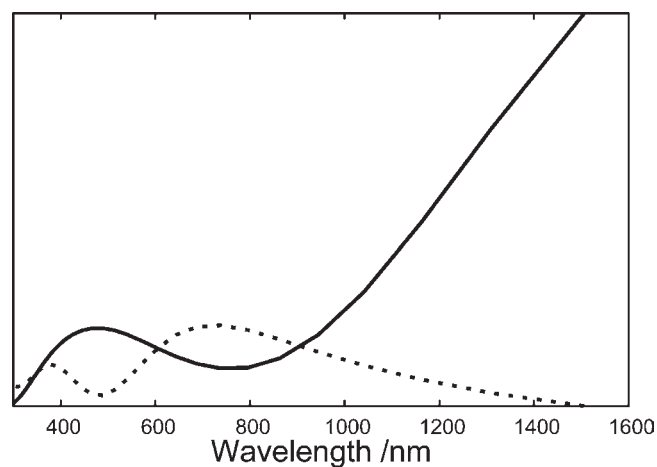


Figure 6. Absorbance spectra (in arbitrary units) of the dry or solvated electron (solid line) and hole (dashed line) in $[N_{1113}][Tf_2N]$. The spectrum was obtained by convolution of the dielectric response function with a Gaussian function of 1 eV fwhm. The spectrum (in nm) was obtained by multiplying the convoluted response function by the frequency.

frequencies probed experimentally. Therefore, the computed UV spectrum (solid line in Figure 6) corresponds to transitions that are solely due to excitations of the dry excess electron. This is an important technical consideration, since pure DFT underestimates the excess electron HOMO–1/HOMO gap (associated with the HOMO/LUMO gap of the neutral system). Even though our computed excess-electron HOMO–1/HOMO gap is probably smaller than the real gap, the computed spectrum is not affected by this underestimation because the HOMO–1 state is involved in excitations of energies larger than the gap, which for this system and within DFT-PBE exceeds 5 eV, thus leading to optical features below 200 nm. In fact, we recomputed this spectrum using a scissors operator that shifts the conduction band levels to match the gap obtained in all-electron periodic B3LYP calculations, and the resulting spectrum was identical. The broadening we used to generate the curves of Figure 6 (1 eV fwhm) was selected on the basis of available estimates^{35–37} for thermal and electronic broadenings observed in other systems as well as from our own observation of the difference in energy of electronic states in the crystalline and liquid phases of our RTILs (see above). We emphasize once again that whereas the liquid is transparent at $t = 0$ in this energy regime and only transitions from the dry electron or hole can take place, this is not the case at later times when chemistry has taken place and different absorbing radicals or other reaction products can contribute to the spectrum. Recent experimental results exploring the transient near-IR spectroscopy of excess electrons in $[N_{1113}][Tf_2N]$ with femtosecond resolution bear resemblance to our calculated results presented in Figure 6, supporting the assertion that our preparation of initial states for these calculations provides a reasonable model of the early-time transient dry electron species.⁴⁴

The results in section 3.1 clearly demonstrate that the dry excess electron in $[mmim][Cl]$ has a pattern of localization that is qualitatively different from those in the other RTILs considered here. In one case, the dry excess electron is delocalized over the π system of the cations, while in all other cases it is delocalized over a group of anions. It is therefore interesting

that the experimental absorption spectra measured for different RTILs exhibit the same qualitative features. According to our calculations and in the absence of other absorbing species, such similarities can be rationalized in the following terms.

Independent of the identity of the RTIL, there are M (where M is the number of ion pairs) electronic states that are similar in nature to the dry excess electron HOMO. These M anionic states in the case of $[N_{1113}][Tf_2N]$, or cationic states in the case of $[mmim][Cl]$, differ mostly in regard to their localization in the liquid. Transitions between states that are similar in character and span an ample range of transition energies give rise to the broad band at low energies and correspond to *translational electronic transitions* of the dry excess electron. By this we mean that upon excitation in this energy range, the final state of the electron is almost indistinguishable from the original except for a spatial translation. In contrast, in both systems, the transitions in the higher-energy UV band (leftmost peak in Figure 6) should correspond to excitations that promote the electron to a state that is qualitatively different in character. In some cases, such as in $[N_{1113}][Tf_2N]$, this state is localized on ions of the opposite charge.

The origin of the two absorbance peaks deserves further scrutiny since it has been shown experimentally⁵ that in the case of $[N_{1444}][Tf_2N]$, their lifetimes are significantly different. Wishart suggested⁵ that the band at high energy has two time constants for decay, one that matches the lifetime of the excess electron and another that does not. Because of this, it has been suggested that this band may correspond in part to absorption due to holes created by ionization of the anions, turning them into radicals.

The computed spectrum of a dry excess hole in neat $[N_{1113}][Tf_2N]$ is shown by the dashed line in Figure 6. For consistency, we used the same liquid geometry as in the case of the excess electron calculation. As can be observed, the hole absorbance leads to a peak below 400 nm and a broader and larger band at ~ 750 nm. The rationalization of the origin of these two bands is analogous to that of the dry excess electron. Promotion of the hole into nearby states of lower energy belonging to the same HOMO band generates radicals of similar character but located in different regions of the liquid. On the other hand, the high-energy part of the spectrum (below 400 nm) is associated with transitions of the hole to states of significantly lower energy in lower-lying bands. While the spectrum of the hole is more prone to the self-interaction error present in the DFT-PBE approach used in our computations, our findings support the observation that the band at low energy (~ 1600 nm) should show a single exponential decay, as it corresponds to the absorption of only one species, namely, the excess electron. On the other hand, the peak at higher energies has contributions both from the excess electron and the excess hole, which as different chemical species very likely decay at different rates.

4. CONCLUSIONS

In this study, we have investigated the electronic structure of several different RTILs in the presence and absence of a dry excess electron. Perhaps one of the most striking findings is that excess electrons do not necessarily localize on or close to cations; instead, their pattern of localization is defined by the relative alignment of cationic and anionic HOMO/LUMO gaps. This means that dry electrons are localized sometimes on anions and

sometimes on cations, depending on the chemical nature of the ions. This opens a window of opportunity for the design of RTILs with varied excess-electron chemistries. It is likely that systems containing the $[\text{Cl}^-]$ anion will be prone to localization of the excess electron on the cations, since the anion HOMO/LUMO gaps are very large.

The dry excess electron HOMO is located at the bottom of an energy band of states with identical character. Transitions between these states give rise to the generic broad low-energy peak observed in our computed spectrum. The smaller peak at higher energies appears to have multiple origins: (1) a dry excess electron can be promoted to a higher band of different character (possibly but not necessarily always located on the counterions) and (2) a dry hole can be promoted down. In the case of $[\text{N}_{1113}][\text{Tf}_2\text{N}]$, the hole also has two absorbance bands. The one at lower energies (but higher than the band of the excess electron) is due to excitation of the hole into lower levels of similar character, while the higher-energy peak is due to excitations to lower-lying energy bands.

Many interesting questions arise from our study. We would like to obtain a better understanding of the effect of quenchers on the absorbance spectrum, the fate of excess electrons upon ionic reorganization, and the key elements governing the relative alignment of cationic and anionic states in the condensed phase. Some of these studies are underway and will be the subject of future publications.

■ ASSOCIATED CONTENT

S Supporting Information. Line and broadened dielectric functions, sample cluster and liquid coordinate files, and complete ref 34. This material is available free of charge via the Internet at <http://pubs.acs.org>.

■ AUTHOR INFORMATION

Corresponding Author

claudio-margulis@uiowa.edu

■ ACKNOWLEDGMENT

C.J.M. acknowledges support by the U.S. Department of Energy, Office of Basic Energy Sciences, Division of Chemical Sciences, Geosciences, and Biosciences under SISGR Grant DE-FG02-09ER16118. C.J.M. also acknowledges the SimBioMa Programme of the European Science Foundation for support of his sabbatical visit to Belfast and Dublin. D.C. acknowledges support from his Science Foundation Ireland Stokes Professorship. We also thank Dr. James Wishart, Prof. Ruth Lynden-Bell, Prof. Patricia Hunt, Dr. Tristan Youngs, Ms. Nancy C. Forero Martínez, and Mr. Daniel Montemayor for insightful discussions. M.G.D.P. and J.K. acknowledge support from the Queen's University Ionic Liquids Laboratory (QUILL).

■ REFERENCES

- (1) Wishart, J. F.; Shkrob, I. A. *ACS Symp. Ser.* **2009**, *1030*, 119–134.
- (2) Ohno, E. H. *Electrochemical Aspects of Ionic Liquids*; Wiley: Hoboken, NJ, 2005.
- (3) Wishart, J. F.; Neta, P. *J. Phys. Chem. B* **2003**, *107*, 7261–7267.
- (4) Grodkowski, J.; Neta, P.; Wishart, J. F. *J. Phys. Chem. A* **2003**, *107*, 9794–9799.
- (5) Wishart, J. F. *ACS Symp. Ser.* **2003**, *856*, 381–396.

- (6) Asano, A.; Yang, J. F.; Kondoh, T.; Norizawa, K.; Nagaishi, R.; Takahashi, K.; Yoshida, Y. *Radiat. Phys. Chem.* **2008**, *77*, 1244–1247.
- (7) Behar, D.; Gonzalez, C.; Neta, P. *J. Phys. Chem. A* **2001**, *105*, 7607–7614.
- (8) Behar, D.; Neta, P.; Schultheisz, C. *J. Phys. Chem. A* **2002**, *106*, 3139–3147.
- (9) Funston, A. M.; Wishart, J. F. *ACS Symp. Ser.* **2005**, *901*, 102–116.
- (10) Kondoh, T.; Asano, A.; Yang, J. F.; Norizawa, K.; Takahashi, K.; Taguchi, M.; Nagaishi, R.; Katoh, R.; Yoshida, Y. *Radiat. Phys. Chem.* **2009**, *78*, 1157–1160.
- (11) Lall-Ramnarine, S. I.; Castano, A.; Subramaniam, G.; Thomas, M. F.; Wishart, J. F. *Radiat. Phys. Chem.* **2009**, *78*, 1120–1125.
- (12) Marcinek, A.; Zielonka, J.; Gebicki, J.; Gordon, C. M.; Dunkin, I. R. *J. Phys. Chem. A* **2001**, *105*, 9305–9309.
- (13) Shkrob, I. A.; Chemerisov, S. D.; Wishart, J. F. *J. Phys. Chem. B* **2007**, *111*, 11786–11793.
- (14) Takahashi, K.; Sato, T.; Katsumura, Y.; Yang, J. F.; Kondoh, T.; Yoshida, Y.; Katoh, R. *Radiat. Phys. Chem.* **2008**, *77*, 1239–1243.
- (15) Yang, J. F.; Kondoh, T.; Norizawa, K.; Nagaishi, R.; Taguchi, M.; Takahashi, K.; Katoh, R.; Anishchik, S. V.; Yoshida, Y.; Tagawa, S. *Radiat. Phys. Chem.* **2008**, *77*, 1233–1238.
- (16) Takahashi, K.; Suda, K.; Seto, T.; Katsumura, Y.; Katoh, R.; Crowell, R. A.; Wishart, J. F. *Radiat. Phys. Chem.* **2009**, *78*, 1129–1132.
- (17) Shkrob, I. A. *J. Phys. Chem. B* **2010**, *114*, 368–375.
- (18) Shkrob, I. A.; Marin, T. W.; Chemerisov, S. D.; Wishart, J. F. *J. Phys. Chem. B* **2011**, *115*, 3872–3888.
- (19) Wang, Z. P.; Zhang, L.; Chen, X. H.; Cukier, R. I.; Bu, Y. X. *J. Phys. Chem. B* **2009**, *113*, 8222–8226.
- (20) Wang, Z. P.; Zhang, L.; Cukier, R. I.; Bu, Y. X. *Phys. Chem. Chem. Phys.* **2010**, *12*, 1854–1861.
- (21) Henderson, W. A.; Fylstra, P.; De Long, H. C.; Trulove, P. C.; Parsons, S. *Phys. Chem. Chem. Phys.* **2011** submitted for publication.
- (22) Del Pópolo, M. G.; Lynden-Bell, R. M.; Kohanoff, J. *J. Phys. Chem. B* **2005**, *109*, 5895–5902.
- (23) Artacho, E.; Anglada, E.; Diéguez, O.; Gale, J. D.; García, A.; Junquera, J.; Martín, R. M.; Ordejón, P.; Pruneda, J. M.; Sánchez-Portal, D.; Soler, J. M. *J. Phys.: Condens. Matter* **2008**, *20*, No. 064208.
- (24) Soler, J. M.; Artacho, E.; Gale, J. D.; García, A.; Junquera, J.; Ordejón, P.; Sánchez-Portal, D. *J. Phys.: Condens. Matter* **2002**, *14*, 2745–2779.
- (25) Perdew, J. P.; Burke, K.; Ernzerhof, M. *Phys. Rev. Lett.* **1996**, *77*, 3865–3868.
- (26) Lee, C. T.; Yang, W. T.; Parr, R. G. *Phys. Rev. B* **1988**, *37*, 785–789.
- (27) Becke, A. D. *Phys. Rev. A* **1988**, *38*, 3098–3100.
- (28) Becke, A. D. *J. Chem. Phys.* **1993**, *98*, 5648–5652.
- (29) Guidon, M.; Schiffmann, F.; Hutter, J.; VandeVondele, J. *J. Chem. Phys.* **2008**, *128*, No. 214104.
- (30) Guidon, M.; Hutter, J.; VandeVondele, J. *J. Chem. Theory Comput.* **2009**, *5*, 3010–3021.
- (31) VandeVondele, J.; Sprik, M. *Phys. Chem. Chem. Phys.* **2005**, *7*, 1363.
- (32) Frigato, T.; VandeVondele, J.; Schmidt, B.; Schütte, C.; Jungwirth, P. *J. Phys. Chem. A* **2008**, *112*, 6125–6133.
- (33) Mantz, Y. A.; Gervasio, F. L.; Laino, T.; Parrinello, M. *J. Phys. Chem. A* **2007**, *111*, 105–112.
- (34) Frisch, M. J.; et al. *Gaussian 03*, revision D.01; Gaussian, Inc.: Wallingford, CT, 2004.
- (35) Hunt, P.; Sprik, M.; Vuilleumier, R. *Chem. Phys. Lett.* **2003**, *376*, 68–74.
- (36) Hunt, P.; Sprik, M. *ChemPhysChem* **2005**, *6*, 1805–1808.
- (37) Neumann, S.; Einfeld, W.; Sobolewski, A. L.; Domcke, W. *J. Phys. Chem. A* **2006**, *110*, 5613–5619.
- (38) Shkrob, I. A.; Wishart, J. F. *J. Phys. Chem. B* **2009**, *113*, 5582–5592.
- (39) Berthon, L.; Nikitenko, S. I.; Bisel, I.; Berthon, C.; Faucon, M.; Saucrotte, B.; Zorz, N.; Moisy, P. *Dalton Trans.* **2006**, 2526–2534.

(40) Bosse, E.; Berthon, L.; Zorz, N.; Monget, J.; Berthon, C.; Bisel, I.; Legand, S.; Moisy, P. *Dalton Trans* **2008**, 924–931.

(41) Le Rouzo, G.; Lamouroux, C.; Dauvois, V.; Dannoux, A.; Legand, S.; Durand, D.; Moisy, P.; Moutiers, G. *Dalton Trans*. **2009**, 6175–6184.

(42) Katoh, R.; Yoshida, Y.; Katsumura, Y.; Takahashi, K. *J. Phys. Chem. B* **2007**, *111*, 4770–4774.

(43) Chandrasekhar, N.; Schalk, O.; Unterreiner, A. N. *J. Phys. Chem. B* **2008**, *112*, 15718–15724.

(44) Ye, M.; Iwata, K. Formation of Solvated Electrons in Tmpa-[Tf2n] Observed with Femtosecond Time-Resolved Near-Infrared Spectroscopy. Presented at the Fourth Congress on Ionic Liquids, Arlington, VA, June 15–18, 2011.